MAGNETOHYDRODYNAMICS Vol. 54 (2018), No. 4, pp. 333–342
DOI: 10.22364/mhd.54.4.1

STALLING INSTABILITY OF ANNULAR LINEAR INDUCTION PUMPS

Linards Goldsteins[1], *Leonids Buligins*[1], *Yves Fautrelle*[2]

[1] *Institute of Physics, University of Latvia, 32 Miera str., LV-2169 Salaspils, Latvia*
[2] *Grenoble INP, SIMAP/EPM Laboratory, Domaine Universitaire, BP 38402, Saint Martin d'Hères, France*
e-Mail: Linards.Goldsteins@lu.lv

In this paper, we analyze stalling instability in the ideal annular linear electromagnetic induction pump (ALIP) coupled with a generalized external load as a power function of the flowrate. It is shown that the stalling threshold in terms of the magnetic Reynolds number Rm will strongly differ depending on the nature of the hydraulic load. It is elucidated why stalling instability can play a key role as a transition phenomenon from stable regime to MHD instability in industrial ALIPs with a sufficiently large Rm.

Introduction. In the context of the French 4$^{\text{th}}$ generation Sodium Fast Reactors (SFR) research and development program for ASTRID (Advanced Sodium Technological Reactor for Industrial Demonstration), a study on the use of high discharge ALIP in the secondary cooling loops has been launched and reported in [1, 2]. Existing examples of ALIP used in SFRs, as well as experimental installations of similar scale have been reported by Andreev *et al.* in [3] and recently by Ota *et al.* in [4] showing that such technology is feasible. Still, several undesirable effects are known to be present in ALIPs.

First, double supply frequency (DSF) pressure oscillations which are a purely electromagnetic end effect and, as shown by Araseki *et al.* [5, 6], can be resolved by using linear grading of the applied magnetic field.

Secondly, the instability of the mean flow which by analogy with asynchronous machine theory can be referred to as stalling instability. The importance of this effect is mentioned by Gailitis *et al.* in [7] and depends on the regime of the coupled pump-load system. It can occur if the pump is overloaded, i.e. the external load is too high, characterized by a sharp decrease of the flowrate and developed pressure.

Finally, MHD instability or the loss of the uniform flow in the pumps channel. This effect is also a consequence of the overloaded ALIP and, as shown later, in some cases could be triggered by the stalling instability. Theoretical and experimental works of Kirillov *et al.* [8, 9] and of Araseki *et al.* [10, 11] show that MHD instability is characterized by a strong vortical flow in the ALIP channel, by the low frequency fluctuations of electrical parameters and pressure, by vibrations and pressure losses.

In the presented paper, we consider only the problem of mean flow or stalling instability of the ALIP-load system. Section 1 is devoted to the description of the ideal ALIP-load system. In section 2, an analysis of the stalling instability of the ALIP coupled with different hydraulic loads is made. Concluding remarks are provided in end of the paper.

1. Quasi-stationary state of an ideal ALIP-external load system. Let us consider a simple system of the pump and external load. The operating point is reached when the developed pressure of the pump Δp is in equilibrium

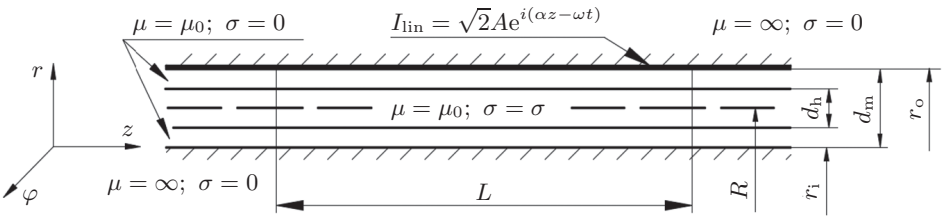

Fig. 1. A model of the ideal ALIP.

with the load pressure Δp_1 (e.g., the pressure drop in the hydraulic circuit), where both are the function of the flowrate Q:

$$\Delta p(Q) = \Delta p_{\text{L}}(Q) \tag{1}$$

To determine the developed pressure of the ideal ALIP, $\Delta p(Q)$, we consider a cylindrical coordinate system (see Fig. 1), where a cylindrical layer of liquid metal of conductivity σ, height d_{h} and mean radius R is moving axially with a velocity v in the annular non-magnetic gap of height d_{m} between two infinitely long, coaxial, perfect ferromagnetic cylinders with the inner and outer radii r_{i} and r_{o}.

A sheet layer of external linear current density I_{lin} is spread on the surface of the external cylinder in the form of a travelling wave with the effective value A, angular frequency ω and wavenumber α:

$$I_{\text{lin}} = \sqrt{2}A \cdot \mathrm{e}^{i(\alpha z - \omega t)}\mathbf{e}_{\varphi} \tag{2}$$

Expression (2), due to Amperes law, defines the boundary condition of the axial magnetic field on the surface of the inductor:

$$B_z|_{r=r_{\text{o}}} = \mu_0 I_{\text{lin}} \tag{3}$$

To derive a height-averaged solution of the problem, let us consider the induction equation for the radial component of the magnetic field:

$$\frac{\partial^2(rB_r)}{\partial r^2} + \frac{\partial^2 B_r}{\partial z^2} - \mu_0\sigma\left(\frac{d_{\text{h}}}{d_{\text{m}}}\right)\left[\frac{\partial B_r}{\partial t} + v\frac{\partial B_r}{\partial z}\right] = 0. \tag{4}$$

By averaging equation (4) over the height, a height-averaged magnetic field radial component $\overline{B}_r$ is introduced:

$$\frac{1}{d_{\text{m}}} \cdot \frac{\partial(rB_r)}{\partial r}\bigg|_{r=r_{\text{i}}}^{r=r_{\text{o}}} + \frac{\partial^2\overline{B}_r}{\partial z^2} - \mu_0\sigma\left(\frac{d_{\text{h}}}{d_{\text{m}}}\right)\left[\frac{\partial\overline{B}_r}{\partial t} + v_z\frac{\partial\overline{B}_r}{\partial z}\right] = 0. \tag{5}$$

Using the magnetic field divergence (6) in expression (5) and applying the boundary condition (3), the height-averaged induction equation from the magnetic field radial component (7) reads as

$$\frac{\partial(rB_r)}{\partial r} = -\frac{\partial B_z}{\partial z} \tag{6}$$

$$\frac{\partial^2\overline{B}_r}{\partial z^2} - \mu_0\sigma\left(\frac{d_{\text{h}}}{d_{\text{m}}}\right)\left[\frac{\partial\overline{B}_r}{\partial t} + v\frac{\partial\overline{B}_r}{\partial z}\right] = i\alpha\mu_0\frac{\sqrt{2}A}{d_{\text{m}}} \tag{7}$$

Searching for a solution in complex form similar to expression (2) yields

$$\overline{B}_r = B \cdot \mathrm{e}^{i(\alpha z - \omega t)}. \tag{8}$$

Substituting expression (8) into the induction equation (7), after derivation, the complex amplitude of the magnetic field is found as

$$B = \frac{B_0}{i + \mathrm{Rm_s}} \tag{9}$$

For the sake of simplicity, the amplitude of the external magnetic field B_0 (10) and the slip magnetic Reynolds number $\mathrm{Rm_s}$ (11) are introduced:

$$B_0 = \frac{\mu_0 \sqrt{2} A}{d_\mathrm{m} \alpha} \tag{10}$$

$$\mathrm{Rm_s} = \mathrm{Rm} \cdot s \tag{11}$$

The magnetic Reynolds number Rm and the slip s are defined in the following way:

$$\mathrm{Rm} = \frac{\mu_0 \sigma v_B}{\alpha} \left(\frac{d_\mathrm{h}}{d_\mathrm{m}} \right) \tag{12}$$

$$s = 1 - \frac{v}{v_B} = 1 - \frac{Q}{2\pi R d_\mathrm{h} v_B} \tag{13}$$

The synchronous velocity of the magnetic field v_B is also introduced as

$$v_B = \frac{\omega}{\alpha} \tag{14}$$

The height-averaged induced currents can be found using Amperes law:

$$\mathbf{j} = j \cdot \mathrm{e}^{i(\alpha z - \omega t)} \mathbf{e}_\varphi = \left[\frac{1}{\mu_0} \cdot \frac{\partial \overline{B}_r}{\partial z} - \frac{I_\mathrm{lin}}{d_\mathrm{m}} \right] \mathbf{e}_\varphi = -\frac{\mathrm{Rm_s}}{i + \mathrm{Rm_s}} \cdot \frac{\sqrt{2} A}{d_\mathrm{m}} \cdot \mathrm{e}^{i(\alpha z - \omega t)} \mathbf{e}_\varphi \tag{15}$$

Finally, we calculate the developed pressure of the ALIP by assuming the inertia of the load to be sufficiently high and by using a quasi-stationary approximation:

$$\Delta p = \Re\mathrm{e} \left\{ \frac{j B^*}{2} \right\} \frac{V}{S} \cdot \frac{\mathbf{e}_\varphi \times \mathbf{e}_r}{\mathbf{e}_z} \tag{16}$$

where V is the volume and S is the surface cross-section of the pump channel.

Using the complex amplitudes from expressions (9) and (15) in equation (16) yields a relatively simple formula of the developed pressure:

$$\Delta p = \frac{\sigma B_0^2 v_B L}{2} \cdot \frac{s}{1 + \mathrm{Rm_s^2}} \tag{17}$$

Next, we introduce a generalized expression of the load pressure (18) which covers not only typical hydraulic loads known from Idelchik [12], but also loads from other classes. In expression (18) it is assumed that the external load Δp_L can be described as a power function, where the coefficients C_n and n depend on the nature of the load as

$$\Delta p_\mathrm{L}(Q) = C_n |Q|^n \operatorname{sign}(Q) \tag{18}$$

In this paper, we consider only positive flowrates, which, as will be shown below, is sufficient for analysis. Then we can simplify as

$$|Q|^n \operatorname{sign}(Q) = Q^n.$$

In praxis, the most common hydraulic loads are cases with $n = 0, 1, 2$:

• If $n = 0$, then $\Delta p_{\mathrm{L}} = C_0$. This can be interpreted as an oppositely applied static pressure head (e.g., created by a container and positioned above the pump) independent of the flowrate and thus neglecting the friction/hydraulic resistance.

• If $n = 1$, then $\Delta p_{\mathrm{L}} = C_1 Q$. This case represents a linear relationship of the pressure drop to the flowrate which is true in laminar flows (Hagen–Poiseuille law). Another example, particularly important in flows of electrically conducting fluids, is the pressure drop caused by the applied magnetic field in case of low magnetic Reynolds numbers.

• If $n = 2$, then $\Delta p_{\mathrm{L}} = C_2 Q^2$. The quadratic relationship of the pressure drop to the flowrate is known to be true in fully turbulent flows with a large Reynolds number as a Darcy-Weisbach equation. This is a common case in the context of liquid metal flows.

For the sake of simplicity, we do not consider the internal resistance of the pump itself in expression (17). It is considered in expression (18), i.e. the estimation of the hydraulic load of the entire circuit. It is done with an assumption that the internal resistance of the pump obeys the same hydraulic resistance law as the external load. This is usually true in praxis, since the Reynolds number is of the same magnitude.

Before we continue with the stability analysis of the mean flow, it is purposeful to introduce dimensionless forms of expressions (17) and (18). First, the dimensionless flowrate is defined in the following way:

$$\widetilde{Q} = \frac{Q}{2\pi R d_{\mathrm{h}} v_B} \tag{19}$$

Then the load pressure drop reads as

$$\Delta p_{\mathrm{L}} = \left[C_n \cdot (2\pi R d_{\mathrm{h}} v_B)^n\right] \cdot \widetilde{Q}^n = K_n \widetilde{Q}^n \tag{20}$$

Choosing the characteristic scale of the pressure dimensionless load and electromagnetic pressure yields:

$$\Delta\widetilde{p}_{\mathrm{L}}(\widetilde{Q}) = \widetilde{Q}^n / \mathrm{N_s} \tag{21}$$

$$\Delta\widetilde{p}(\widetilde{Q}) = \frac{1 - \widetilde{Q}}{1 + \mathrm{Rm}^2\left(1 - \widetilde{Q}\right)^2} \tag{22}$$

where the systems integral interaction parameter $\mathrm{N_s}$ characterizes the ratio of electromagnetic and load forces or pressure drops as

$$\mathrm{N_s} = \frac{\sigma B_0^2 v_B L}{2K_n} \tag{23}$$

2. Stability of mean flow in the ideal ALIP. To analyze the mean flow stability in the pump-load system, the stability condition has been proposed by Gailitis *et al.* in [7]. It states that the operating point is instable if the slope of the pressure-flowrate characteristic of the pump is steeper than that of the load, or mathematically it reads as

$$\frac{\partial\left(\Delta\widetilde{p}\right)}{\partial\widetilde{Q}} > \frac{\partial\left(\Delta\widetilde{p}_{\mathrm{L}}\right)}{\partial\widetilde{Q}} \tag{24}$$

Using expressions (21) and (22) in condition (24) we have:

$$\mathrm{N_s} \cdot \frac{\partial\left(\dfrac{1 - \widetilde{Q}}{1 + \mathrm{Rm}^2(1 - \widetilde{Q})^2}\right)}{\partial\widetilde{Q}} > \frac{\partial\left(\widetilde{Q}^n\right)}{\partial\widetilde{Q}}. \tag{25}$$

We derive the interaction parameter $\mathrm{N_s}$ from the pressure equilibrium at the operating point:

$$\Delta\widetilde{p} = \Delta\widetilde{p}_{\mathrm{L}} \quad \rightarrow \quad \mathrm{N_s} = \frac{\widetilde{Q}^n \left(1 + \mathrm{Rm_s^2}\right)}{1 - \widetilde{Q}}. \tag{26}$$

Then substituting expression (26) into expression (25) after derivation yields:

$$\frac{\widetilde{Q}^n \left(\mathrm{Rm_s^2} - 1\right)}{\left(1 - \widetilde{Q}\right)\left(1 + \mathrm{Rm_s^2}\right)} - n\widetilde{Q}^{n-1} > 0. \tag{27}$$

From expression (27) the condition for the critical Rm is found as

$$\mathrm{Rm} > \frac{1}{1 - \widetilde{Q}} \sqrt{\frac{n + (1-n)\widetilde{Q}}{(n+1)\,\widetilde{Q} - n}} \tag{28}$$

Using condition (28) in equation (26) the critical N_s can be also derived.

Let us reduce the analysis to three previously described cases when $n = [0, 1, 2]$. It follows that

• If $n = 0$, the stability of the mean flow will be lost as soon as the critical $\mathrm{Rm_s}$ is reached:

$$\mathrm{Rm} > \frac{1}{1 - \widetilde{Q}} \quad \rightarrow \quad \mathrm{Rm_s} > 1 \tag{29}$$

Condition (29) is satisfied when exceeding the maximum point of the p-Q curve governed by Eq. (22) and leads to the stop of the pump similarly as of the overloaded asynchronous motor, since above this limit there is no operating point which satisfies Eq. (1).

• If $n = 1$, the laminar flow is considered in the hydraulic circuit. Using expression (28), the critical Rm as a function of the flowrate reads

$$\mathrm{Rm} > \frac{1}{1 - \widetilde{Q}} \sqrt{\frac{1}{2\widetilde{Q} - 1}} \tag{30}$$

Real values of are found for the flowrates $\widetilde{Q} = 0.5 \ldots 1$, then by estimating the $\mathrm{Rm_s}$ and $\mathrm{N_s}$s, the curves of the critical Rm and $\mathrm{N_s}$s as functions of $\mathrm{Rm_s}$ are illustrated in Fig. 2.

From the curves in Fig. 2 it can be seen that in the case of laminar flow in the circuit, the necessary conditions for stalling instability to occur are $\mathrm{Rm} > 5.2$, $\mathrm{N_s} > 8$ and $\mathrm{Rm_s} > 1$. Using these curves, critical values of $\mathrm{N_s}$ and $\mathrm{Rm_s}$ for the ALIP operating with a fixed Rm, e.g., $\mathrm{Rm} = 8$, are estimated.

In Fig. 3, an overcritical ALIP ($\mathrm{Rm} = 8$) coupled with the hydraulic loop is shown. Interaction parameters of different systems are varied by varying the loops hydraulic resistance, e.g., by using a valve. One can see that with the interaction parameter $\mathrm{N_s} = 13.8, 17.1$, lines 2 and 4 are tangent to the ALIP characteristic at points 4 and 2, respectively. Any other point between points 2 and 4 is instable, meaning that it is impossible operate the ALIP in this zone.

Let us consider the operation of such system by starting at the stable point 1 ($\mathrm{N_s} = 17.1$) in Fig. 3. When shutting the valve (so decreasing $\mathrm{N_s}$), the stable operation is maintained until point 2 is reached $\mathrm{N_s} = 13.8$. From this point, the system will instantaneously jump to the stable point 3, greatly decreasing the developed pressure and flowrate. When trying to restore the previous state by opening the valve (increasing $\mathrm{N_s}$) from point 3 reaching the instable point 4

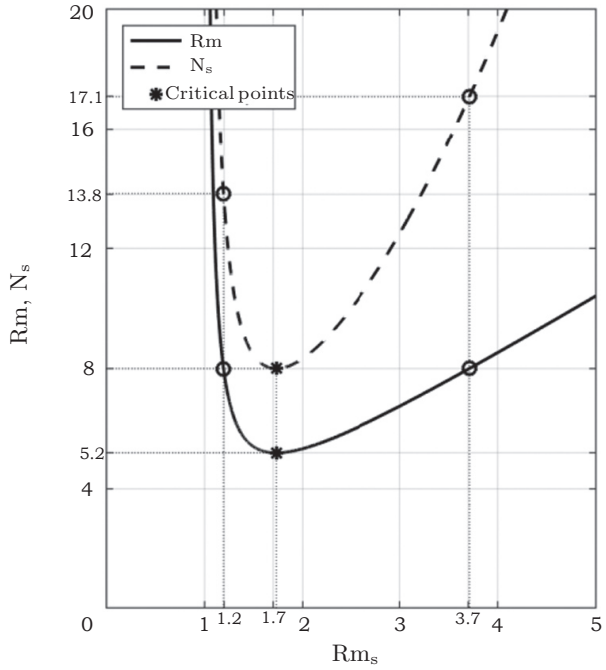

Fig. 2. Critical curves of Rm and N_s, $n = 1$.

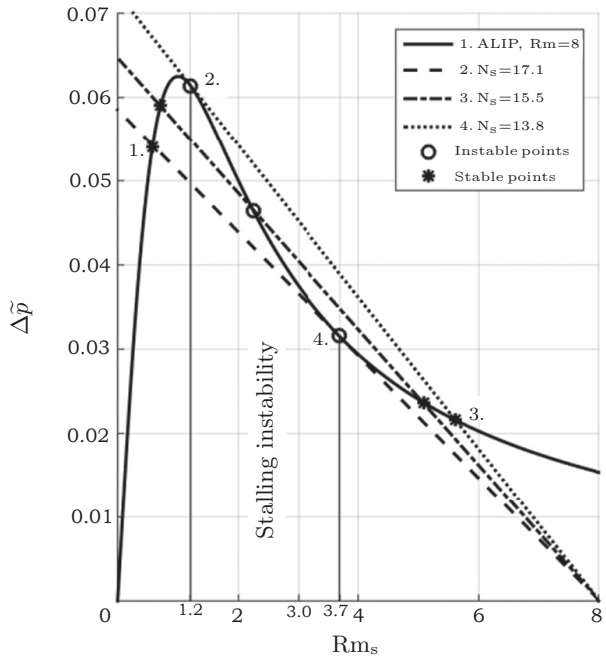

Fig. 3. Characteristic of the ideal ALIP coupled with external loads: Rm = 8, $n = 1$.

($N_s = 17.1$), the system will experience a sharp transition back to the stable point 1. Such hysteresis type behaviour $1 \ldots 2 \to 3 \ldots 4 \to 1$ gives evidence that the ALIP does not operate in the zone between points 2 and 4.

A qualitatively similar behaviour and hysteresis of the ALIP performance has been observed in a numerical work of Gissinger *et al.* [13].

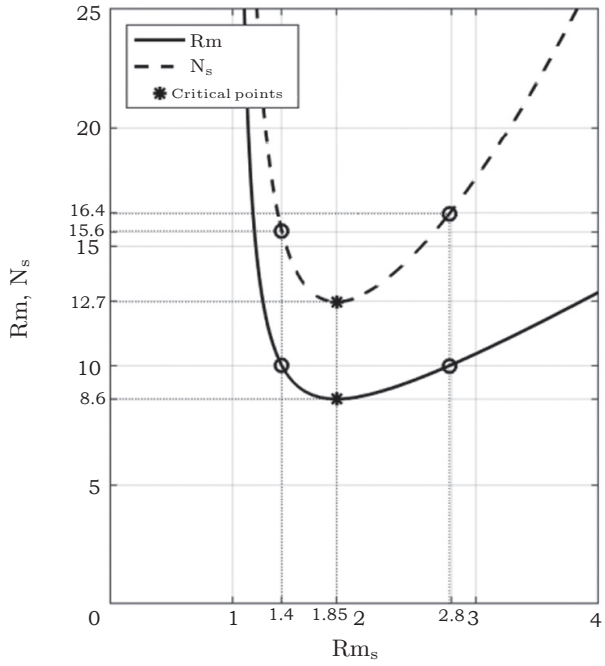

Fig. 4. Critical curves of Rm and N_s, $n = 2$.

• If $n = 2$, the turbulent flow is assumed in the hydraulic circuit, and the following condition form expression (28) is obtained:

$$\mathrm{Rm} > \frac{1}{1-\widetilde{Q}}\sqrt{\frac{2-\widetilde{Q}}{3\widetilde{Q}-2}} \tag{31}$$

The critical N_s and Rm are plotted as a function of Rm_s in Fig. 4.

By analyzing the obtained curves in Fig. 4, it can be pointed out that the critical parameters of the instability to occur exceed 8.6, $N_s > 12.7$ and $Rm_s > 1$, which are higher than in the case of laminar flow. With the increase of Rm, the critical Rm_s decreases to lower values (e.g., $Rm_s \approx 1.4$ at $Rm = 10$).

In Fig. 5, an overcritical ALIP (Rm = 10) coupled with the hydraulic loop is shown. One can observe a similar behaviour as that discussed previously: by changing the interaction parameter $N_s = [15.6, 16.4$, curves 2 and 3 are tangent to the ALIP characteristic at points 2 and 4, respectively. Any other point between points 2 and 4 is instable, meaning that it is impossible operate the ALIP in this region. Points 1 and 3 are stable and a hysteresis similar to the previously described case with $n = 1$ can be expected when the interaction parameter is varied.

Achieving $Rm > 5.2 \ldots 8.6$ is realistic in large, industrial-scale ALIPs using liquid sodium. The described stalling behaviour qualitatively agrees with the experimentally reported behaviour of a large ALIP for SFR by Ota *et al.* [4], where $Rm \approx 6.42$ was estimated and three principal operating areas were identified and are summarized in Fig. 6:

(i) stable homogeneous flow; nominal operation regime;

(ii) transient instability; the operation is impossible in this zone;

(iii) MHD instability; inhomogeneous flow, large fluctuation of the flowrate and pressure; undesirable operation regime.

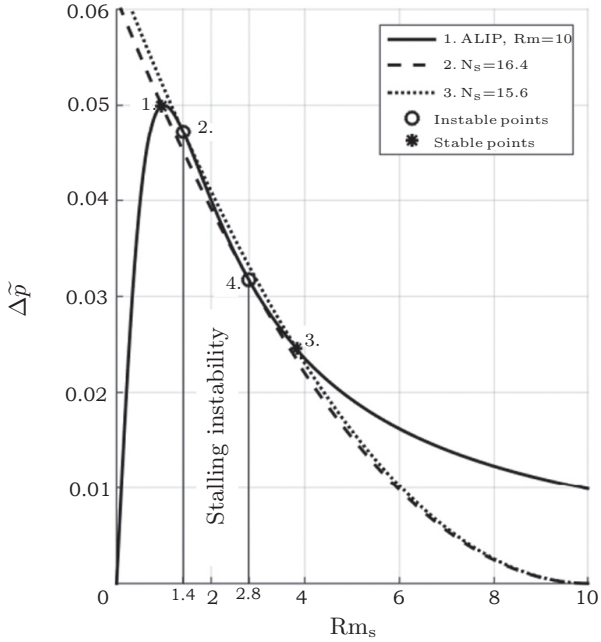

Fig. 5. Characteristic of the ideal ALIP coupled with external loads: $\mathrm{Rm} = 10$, $n = 1$.

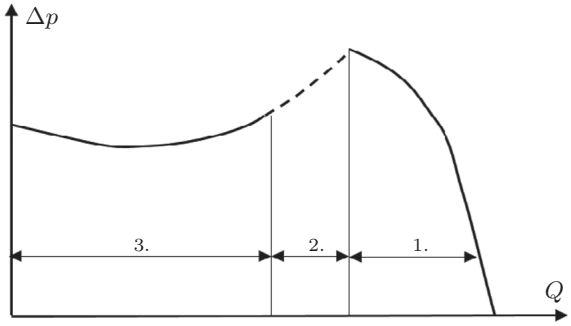

Fig. 6. Classification of large ALIP flow regimes observed in the experiment by Ota *et al.* [4].

In the context of this classification it is reasonable to suggest that area 2 is the region of stalling instability. Apparently, it can play an important role as a trigger or transition mechanism from stable flow to MHD instability governed by the inhomogeneous flow.

3. Summary and conclusions. In this paper, several important aspects of stalling instabilities in the ideal ALIP have been discussed and elaborated in details for the first time.

First, stalling instability thresholds have been found in case of positive flowrates for three typical hydraulic load types – static, linear and quadratic. If the necessary interaction parameters $\mathrm{N_s}$ (electrical current) can be achieved, these thresholds can be summarized in terms of the magnetic Reynolds number Rm as

1. Opposing static pressure (constant pressure drop) $n = 0$: $\mathrm{Rm} > 1$.
2. Laminar flow in the circuit (linear pressure drop) $n = 1$: $\mathrm{Rm} > 5.2$.
3. Turbulent flow in the circuit (quadratic pressure drop) $n = 2$: $\mathrm{Rm} > 8.6$.

The presented stability criterion in expression (28) from which the mentioned thresholds are obtained is generalized and can be used for any arbitrary n, allowing to study other types of hydraulic loads which can be approximated using expression (18). The analysis has shown that the stalling instability can occur only under regimes when $\mathrm{Rm_s} > 1$. If the critical Rm can be reached, the stalling instability in case of laminar flow ($n = 1$) can be expected at $\mathrm{Rm_s} \approx 1 \ldots 1.7$, but in a turbulent flow ($n = 2$) $\mathrm{Rm_s} \approx 1 \ldots 1.85$. It should be emphasized that the higher values of Rm, the lower $\mathrm{Rm_s}$ values are necessary for the stalling to occur.

Secondly, by analyzing the behaviour of stalling instability in the ideal ALIP/load system – changing interaction parameter $\mathrm{N_s}$ (Figs. 3 and 5), it was found that sharp transitions to higher $\mathrm{Rm_s}$ (lower flowrates and pressure) can be expected near the maximum point of the characteristics. Moreover, the system cannot be recovered after the stalling immediately by increasing $\mathrm{N_s}$, but it experiences hysteresis. Only when $\mathrm{N_s}$ (electrical current) is sufficiently increased, the system experiences another sharp recovery transition. Such behaviour indicates that the stalling instability could play an important role as a triggering mechanism in the transition from the stable ALIP operation to flow regimes governed by MHD instability.

The obtained results are significant practically, since the case of turbulent flow ($n = 2$) is typical for liquid metal applications. In ALIPs operating with liquid sodium achieving a threshold $\mathrm{Rm} > 8.6$ is realistic, in particular, in large-scale pumps for SFRs.

In the end, possible solutions to the stalling instability problem in praxis should be mentioned. There are at least two ways to tackle this problem:

(i) Development of an ALIP control feedback loop (by varying the current and the frequency) that the operation point is always at the low slip magnetic Reynolds number $\mathrm{Rm_s} < 1$, independently of the Rm value. A special power supply with a broad operating range is required for this solution.

(ii) Modification of the spatial distribution and type of the applied magnetic field, e.g., by changing winding connections or its temporal behaviour that condition (24) is not satisfied.

The modification of the external field in the ALIP seems to be the most robust way to resolve the instability problem. There is experimental evidence by Araseki *et al.* in [11] that by varying the winding connection a stabilization effect of MHD instability can be achieved up to some extent. By analogy, it is reasonable to suggest that a similar modification could also positively affect the stalling instability. Still, proofs of such assumption are needed, therefore, it is an open question for the future studies.

Acknowledgements. Authors acknowledge financial support of the CEA-UL Collaboration Agreement on ASTRID: V CEA 2017 02 10 in the framework of which this study was conducted.

References

[1] F. Gauche *et al.* French SFR R&D program and design activities for SFR prototype ASTRID. *Anisan Nuclear Prospects 2010*, (2011), pp. 314–316.

[2] G. Rodriguez *et al.* Development of experimental facility platform in support of the ASTRID program. *Proc. International Conference on Fast Reactor and Related Fuel Cycles, 2013*.

[3] A.M. Andreev *et al.* The TsLIN-3/3500 electromagnetic pump. *Magnetohydrodynamics*, vol. 24 (1988), no. 1, pp. 55–61.

[4] H. Ota *et al.* Development of 160 m3/min large capacity sodium-immersed self-cooled electromagnetic pump. *J. Nuclear Science and Technology*, vol. 41 (2004), pp. 511–523.

[5] H. Araseki *et al.* Double-supply-frequency pressure pulsation in annular linear induction pump. Part I: Measurment and numerical analysis. *Nuclear Engineering and Design*, (2000), pp. 85–100.

[6] H. Araseki *et al.* Double-supply-frequency pressure pulsation in annular linear induction pump. Part II: Reduction of pulsation by linear winding grading at both stator ends. *Nuclear Engineering and Design*, (2000), pp. 397–406.

[7] A. Gailitis, O. Lielausis. Instability of homogeneous velocity distribution in an induction-type MHD machine. *Magnetohydrodynamics*, vol. 11 (1975), no. 1, pp. 69-79.

[8] I.R. Kirillov, A.P. Ogorodnikov, V.P. Ostapenko. Experimental investigation of flow nonuniformity in a cylindrical linear induction pump. *Magnetohydrodynamics*, vol. 16 (1080), no. 2, pp. 169-201.

[9] I.R. Kirillov, V.P. Ostapenko. Local characteristics of a cylindrical induction pump for $\mathrm{Rms} > 1$. *Magnetohydrodynamics*, vol. 23 (1987), no. 2, pp. 196–202.

[10] H. Araseki *et al.* Magnetohydrodynamic instability in annular linear induction pump. Part I. Experiment and numerical analysis. *Nuclear Engineering and Design*, (2004), pp. 29–50.

[11] H. Araseki *et al.* Magnetohydrodynamic instability in annular linear induction pump. Part II. Suppression of instability by phase shift. *Nuclear Engineering and Design*, (2006), pp. 965–974.

[12] I.E. Idelchik. *Handbook of Hydraulic Resistance* (Moscow, Mashinostroyeniye Publishing House, 1992) (in Rissian).

[13] C. GissingeR *et al.* Instability in electromagnetically driven flows. Part I. *Physics of Fluids*, vol. 28 (2016), no. 3.

Received 30.10.2018